Loss of CDC50A function drives Aβ/p3 production via increased β/α-secretase processing of APP

Marc D. Tambini & Luciano D'Adamio

Department of Pharmacology, Physiology & Neuroscience New Jersey Medical School, Brain Health Institute, Jacqueline Krieger Klein Center in Alzheimer's Disease and Neurodegeneration Research, Rutgers, The State University of New Jersey, 185 South Orange Ave, Newark, NJ, 07103, USA.

Correspondence to: marc.tambini@rutgers.edu, luciano.dadamio@rutgers.edu

Abstract

The Amyloid Precursor Protein (APP) undergoes extensive proteolytic processing to produce several biologically active metabolites which affect Alzheimer's disease (AD) pathogenesis. Sequential cleavage of APP by β- and γ-secretases results in Aβ, while cleavage by α- and γ-secretases produces the smaller p3 peptide. Here we report that in cells in which the P4-ATPase flippase subunit CDC50A has been knocked out, large increases in the products of β- and α-secretase cleavage of APP (sAPPβ/βCTF and sAPPα/αCTF, respectively) and the downstream metabolites Aβ and p3 are seen. These data indicate that APP cleavage by β/α-secretase are increased and suggest that phospholipid asymmetry plays an important role in APP metabolism and Aβ production.

Introduction

Alzheimer's disease (AD) is the most common form of dementia of the elderly[1]. Familial forms of AD are caused by mutations in the gene encoding the Amyloid Precursor Protein (APP) or in genes encoding Presenilin 1 or 2 (PS1/2), which process fragments of APP to produce plaque-forming Aβ peptides[2, 3]. APP is processed in two main pathways[4]. In the amyloidogenic pathway, APP undergoes sequential cleavage first by β-secretase (BACE1)[5] to produce one large soluble extracellular domain (sAPPβ) and one β-carboxy terminal fragment (βCTF). βCTF is then further processed by γ-secretase, composed in part by PS1 and PS2, to produce one molecule of Aβ and one molecule of APP-intracellular domain (AID/AICD)[6]. In the nonamyloidogenic pathway, APP is first cleaved within the Aβ region by α-secretase, to release a large soluble domain (sAPPα), and one αCTF. αCTF is then processed by γ-secretase to produce one molecule of the nonamyloidogenic p3 and one molecule of AID/AICD. Because metabolites of APP are biologically active and have numerous effects on AD-related histopathology and synaptic function[7, 8], the cellular processes and genes that govern APP processing are of considerable scientific interest.

When considering non-Mendelian, late-onset forms of AD, one of the themes to emerge from the large scale genome-wide association studies is that genes involved in lipid homeostasis[9] are responsible for, as non-deterministic genetic risk factors, the more common forms of AD. The classical and most well-validated example is Apolipoprotein E (ApoE)[10], an extracellular lipid transporter whose AD-associated isotype can significantly increase AD risk. The phosphatidylserine (PtdSer) sensing ability of the microglial protein Triggering Reception in Microglia 2 (TREM2) has been shown to be altered by AD-causing *TREM2* mutations[11]. The PtdSer transporter ATP-binding cassette A7 (ABCA7) likewise is mutated in late-onset AD[12].

Recently, cell division cycle protein 50A (CDC50A, also termed TMEM30A), a subunit of a class of lipid transporters called flippases[13], which transport phospholipids from the

exofacial leaflet of the plasma membrane to the cytosolic face, has been reported to bind βCTF and affect APP-CTF levels in an *in vitro* overexpression model[14]. Given the constitutively active nature of PtdSer flippase activity, it is possible that an over expression paradigm may not reveal the true impact of CDC50A on APP processing, in addition to the possible confounding effects caused by overexpression artifacts. Indeed, the loss of CDC50A function, and therefore a loss of flippase function, has been shown to have a neurodegenerative phenotype in conditional KO models[15, 16], we wished to determine the effect of loss of CDC50A function has on APP processing. Here, we characterize APP processing in a human CDC50A knockout (KO) tumor cell line. We report a significant increase in p3 and Aβ production in CDC50A-KO cells, driven by increase in α- and β-processing of APP and other substrates.

Results

CDC50A loss of function increases Aβ, p3, and sAPP secretion in cultured cells.

CDC50A-KO cells were generated by Horizon Discovery via the CRISPR/Cas9-mediated 16-bair pair deletion in the *CDC50A* coding region of parental wild-type HAP1 cells. RT-PCR of CDC50A RNA demonstrates an 18-fold decrease in CDC50A transcript in CDC50A-KO cells, likely the result of nonsense-mediated decay (Fig 1A). Functional knockout of CDC50A was confirmed by testing surface Annexin V binding, an indirect measure of surface levels of PtdSer. HAP1 cells showed no Annexin V staining, consistent with intact PtdSer flippase activity (Fig. 1B, top panel), whereas CDC50A-KO cells were positive (Fig. 1B, middle panel), indicating increased surface levels of PtdSer. HAP1 cells could be made to robustly expose PtdSer by induction of apoptosis with staurosporine treatment (Fig. 1C, bottom panel). These data indicate that CDC50A-KO cells reproduce the expected loss of function of PtdSer flippase activity.

APP metabolite levels of HAP1 and CDC50A-KO cell conditioned media were determined by ELISA. Two different ELISAs were used to determine Aβ levels: one with the

detection antibody 4G8, which recognizes Aβ amino acids 3-8, and one with detection antibody 6E10, which recognizes Aβ amino acids 17-24. 4G8 therefore detects Aβ and p3, the fragment of APP-CTF that is produced from α- and γ-cleavage, whereas 6E10 only detects Aβ. The difference in 4G8 and 6E10 signal can then be used to calculate the level of p3. Note that in brain homogenates, it has been found that the differing activities of 6E10 and 4G8 are such that p3 cannot be reliably estimated by this method[17], whereas in cultured cells, this method has been shown to be reliable[18, 19]. In cultured media from CDC50A-KO cells, a 9-fold increase in Aβ40 is seen, as detected by 6E10, and a 26-fold increase in the calculated p3(Aβ17-40) as compared to HAP1 conditioned media (Fig. 2A). The longer Aβ42 and p3(Aβ17-42) are also increased in CDC50A-KO conditioned media, at 10-fold and 3-fold respectively (Fig. 2B). Levels of the large soluble ectodomains of APP derived from the α- and β-cleavage of APP, termed sAPPα and sAPPβ respectively, were determined by ELISA of HAP1 and CDC50A-KO conditioned media. Both sAPPα and sAPPβ were found to be significantly increased, at 8-fold and 3-fold, in media from CDC50A-KO cells as compared to controls. Overall, these data indicate the increased α- and β-processing of APP in CDC50A-KO cells.

CDC50A-KO cells show general altered levels of γ-secretase substrates under γ-secretase inhibition.

Given that increased Aβ and p3 levels can be the result of increased γ-secretase activity or increased total substrate levels of the full length APP, we wished to determine membrane bound APP and APP-CTF levels of HAP1 and CDC50A-KO lysates by Western analysis. While a 54% and 57% increase in immature and mature APP were noted in CDC50A-KO cells (Fig. 3A), this increase is not of a sufficient magnitude to explain the manifold increase in Aβ and p3 levels secreted by CDC50A-KO cells. APP-CTFs are likewise unaltered by CDC50A knockout (Fig. 3A). We tested another substrate of γ-secretase, N-cadherin, and found no difference in the levels of full-length N-cadherin and a minor increase in N-cadherin-CTFs (Fig. 3B). Components of γ-secretase itself showed minor alterations, with CDC50A-KO cells having 32%

more PS1-CTF levels (Fig. 3C), 22% lower PS2-CTF levels (Fig. 3D), and 27% increased levels of nicastrin (Fig. 3E). There is no evidence of altered PS1 or PS2 auto-catalysis (Fig. 3C-D), as no full-length PS1 or PS2 is detectable. The data do not support the idea that the changes in Aβ and p3 is the result of altered γ-secretase function.

sAPPα and sAPPβ are better indicators of α- and β-cleavage of APP than levels of αCTF and βCTF, which undergo further processing by various pathways. We wished to determine if the increase in αCTF and βCTF that are predicted by the increases in sAPPα and sAPPβ can be revealed by blocking APP-CTF degradation with a γ-secretase inhibitor. HAP1 and CDC50A-KO cells were treated with compound E, a potent, selective, noncompetitive inhibitor of γ-secretase. Compound E activity was confirmed by the large increase in APP-CTFs seen by Western analysis (Fig. 4A). Interestingly, under γ-inhibition, CDC50A-KO cell lysates had 15-fold higher αCTF and 44-fold higher βCTF than wild-type HAP1 cells (Fig. 4A). This effect is not specific to APP, as N-cadherin-CTFs were also significantly increased in γ-inhibited CDC50A-KO cells under γ-inhibited controls (Fig. 4B). The absence of any difference in APP-CTFs or N-cadherin-CTFs in CDC50A-KO cells in the steady state indicates that γ-secretase can efficiently processes the increased substrates that result from elevated α- and β-activity.

Discussion

In this study, we demonstrate that APP undergoes increased α- and β-cleavage to produce more p3 and Aβ in CDC50A-KO cells. The mechanism of this increased processing is unclear. Loss of membrane phospholipid asymmetry has been reported to have numerous effects on endocytic trafficking. We speculate that this disrupted trafficking would result in the general altered processing of membrane proteins. APP, a type 1 transmembrane protein, is generated in the ER, travels along the biosynthetic pathway to the plasma membrane, and is then endocytosed to late endosome/lysosome. Along this pathway, it is subject to numerous cleavages. At the plasma membrane, APP is predominantly cut by α-secretase, while the acidic

lumen of the late endosome/lysosome favors β-cleavage. Given that both the amyloidogenic and non-amyloidogenic pathways are upregulated in CDC50A-KO cells, it seems unlikely phospholipid asymmetry causes APP mislocalization, or selective organellar dysfunction. Instead, it is possible that there is a generalized increase in membrane turnover, and this idea is supported by the observation that another type-1 transmembrane protein, N-cadherin, was affected in a similar manner.

Materials and Methods

Cell Lines and reagents. Wild-type HAP1 and CDC50A-KO cell lines were purchased from Horizon Discovery (C631, HZGHC005423c009). Cells were cultured in DMEM (Gibco 11995-065), supplemented with 10% FBS (Gibco 26140-079) and 1% antibiotic–antimycotic (Gibco 15240) at 37°C and 5% CO_2. Compound E (EMD Millipore 565790) was used at a final concentration of 10μM for 18h for the γ-secretase inhibited samples. Staurosporine (Cell Signaling 9953) was used at final concentration of 1μM for 2hr to induce apoptosis.

Western Analysis. Cells were grown in a monolayer to 90% confluency, washed 3x in PBS, and scraped off into ice-cold homogenization buffer (20 mM Tris-base pH 7. 4, 250 mM sucrose, 1 mM EDTA, 1 mM EGTA) plus protease/phosphatase inhibitors (ThermoScientific). Cells were lysed via sonication and total protein was measured by Bradford analysis. 10 μg of protein plus LDS Sample buffer/10% β-mercaptoethanol (Invitrogen NP0007) were separate by PAGE on a 4–12% Bis-Tris polyacrylamide gel (Biorad 3450125), transferred onto nitrocellulose using the Trans-blot Turbo system (Biorad) and visualized by red Ponceau staining. After membranes were blocked in 5%-milk (Biorad 1706404), the following primary antibodies were applied overnight at 4°C, at 1:1000 dilution in blocking solution (Thermo 37573): APP-Y188 (Abcam ab32136), PS2 (Cell signaling, 2192), Nicastrin (Cell signaling, 5665), N-cadherin (Cell signaling, 14215), PS1 (Cell signaling, 5643) and GAPDH (Sigma G9545). Either anti-mouse (Southern Biotech 1031-05) or a 1:1 mix of anti-rabbit (Southern Biotech, OB405005) and anti-

rabbit (Cell Signaling, 7074), were diluted 1:1000 in 5% milk and used against mouse and rabbit primary antibodies for 30 min, RT, with shaking. Blots were developed with West Dura ECL reagent (Thermo, PI34076) and visualized on a ChemiDoc MP Imaging System (Biorad). Signal intensity was quantified with Image Lab software (Biorad). Data were analyzed using Prism software and represented as mean ± SD GAPDH (Sigma G9545). After extensive washings in PBS/Tween20 0. 05%, the following secondary antibodies were used diluted 1:1000 in 5%-milk: anti-mouse (Southern Biotech, 1031–05) and a 1:1 mix of anti-rabbit (Southern Biotech, 4050–05) and anti-rabbit (Cell Signaling, 7074). Secondary antibodies were incubated with membranes for 30 min, RT, with shaking). After extensive washings in PBS/Tween20 0. 05%, blots were developed with West Dura ECL reagent (Thermo, PI34076), visualized with ChemiDoc MP Imaging System (Biorad) and signal intensities were quantified with Image Lab software (Biorad).

ELISA. Measurement of Aβ40, Aβ42, sAPPα, and sAPPβ content of conditioned media was preformed using the following Meso Scale Discovery: PLEX Plus Aβ Peptide Panel 1 6E10 (K15200G), V-PLEX Plus Aβ Peptide Panel 1 4G8 (K15199G), sAPPα/sAPPβ (K15120E), according to the manufacturer's recommendations. Fresh media was applied to cells for 24 hours, and dead cells were removed by a 10m, 20,000 x g spin before the supernatant was used for analysis. Plates were read on a MESO QuickPlex SQ 120. Data were analyzed using Prism software and represented as mean ± SD.

RT-PCR. RNA was extracted from cultured cells using the RNeasy RNA Isolation kit (Qiagen 74104) and used as template for cDNA generation with a High-Capacity cDNA Reverse Transcription Kit (Thermo 4368814). Real-time PCR was performed using 50 ng of cDNA and TaqMan Fast Advanced Master Mix (Thermo 4444556). GAPDH mRNA was detected with probe Hs02786624_g1 and CDC50A mRNA was detected with probe Hs01092148_m1 (Thermo). Samples were analyzed on a QuantStudio 6 Flex Real-Time PCR System (Thermo). LinRegPCR software (hartfaalcentrum.nl) was used to quantify relative mRNA amounts.

Annexin V labeling and microscopy. Cells were grown on glass coverslips, washed 3x in PBS and stained with Annexin V-FITC on ice, according to the manufacturer's recommendations (BD Pharmingen 550911). Cells were fixed with 4% paraformaldehyde for 15m at room temperature, washed, mounted onto glass slides and visualized using an Axiovert fluorescence microscope (Zeiss).

Statistical Analysis. Statistical significance was evaluated using the two-sided Student's *t*-test. Statistical analysis was performed with GraphPad Prism v8 for PC. Significant differences were accepted at $p < 0.05$.

Figure Legends

Figure 1. Validation of CDC50A-KO by RT-PCR and PtdSer binding assay. A.) CDC50A RNA was detected in wild-type HAP1 cells and CDC50A-KO cells. Data were analyzed by two-sided Student's *t*-test and represented as mean ± SD. n=4 per genotype, ****p<0.0001. B.) Annexin V-FITC (AnV-FITC) binding was visualized in HAP1, CDC50A-KO, and staurosporine-treated (1µM, 2hr) HAP1 cells by fluorescent microscopy.

Figure 2. ELISA of APP metabolites in WT and CDC50A-KO cell conditioned media. A.) Levels of Aβ40 were determined by ELISAs with either 4G8 (left graph, detects both p3 and Aβ) or 6E10 (middle graph, only detects Aβ) detection antibodies. p3/Aβ17-40 (right graph) was calculated by subtracting 4G8 values from 6E10 values. B.) Levels of Aβ42 were determined by ELISAs with either 4G8 (left graph, detects both p3 and Aβ) or 6E10 (middle graph, only detects Aβ) detection antibodies. p3/Aβ17-42 (right graph) was calculated by subtracting 4G8 values from 6E10 values. C.) Levels of sAPPα and sAPPβ were determined by ELISA. For all ELISAs, data were analyzed by two-sided Student's *t*-test and represented as mean ± SD. n=6 per genotype, *p<0.05, ****p<0.0001.

Figure 3. Western analysis of APP, N-cadherin, and γ-secretase component levels of WT and CDC50A-KO cell lysates. The following antibodies were used to probe wild-type HAP1 and CDC50A-KO cell lysates: A.) Y188 APP C-terminus. Mature and immature full-length APP, and APP-CTFs, both αCTF and βCTF, are indicated. APP-CTFs were quantitated from the darker exposure. B.) N-cadherin C-terminus. Full length N-cadherin and N-cadherin-CTFs are indicated. Full-length N-cadherin was quantitated from the lighter exposure, and N-cadherin-CTFs were quantitated from the darker exposure. Note the band designated as N-cadherin CTF has been experimentally tested (Fig. 4B) and identified as N-cadherin CTF via its sensitivity to γ-secretase inhibition. All other bands are non-specific signals. C.) PS1 C-terminus. PS1-CTF is indicated, with no full length PS1 detected. D.) PS2 C-terminus. PS2-

CTF is indicated, with no full length PS2 detected. E.) Nicastrin. Quantitation is shown at the right or below each blot. All data were normalized to GAPDH signal, analyzed by two-sided Student's t-test, and represented as mean ± SD. n=6 per genotype, *p<0.05, ***p<0.001.

Figure 4. Western analysis of APP and N-cadherin in WT and CDC50A-KO cell lysates under γ-secretase inhibition. Wild-type HAP1 and CDC50A-KO cells were either untreated or treated with compound E, a potent, selective, non-competitive γ-secretase inhibitor. Cell lysates were probed as follows: A.) Y188 APP C-terminus. Mature and immature full-length APP, and APP-CTFs, both αCTF and βCTF, are indicated. APP-CTFs were quantitated from the γ-secretase inhibited samples using the lighter exposure. A darker exposure indicates the degree of γ-secretase inhibition of compound E treated samples. B.) N-cadherin C-terminus. Full length N-cadherin and N-cadherin-CTFs are indicated. N-cadherin-CTFs from the γ-secretase inhibited samples were quantitated from the darker exposure. All data were normalized to GAPDH signal, analyzed by two-sided Student's *t*-test, and represented as mean ± SD. n=3 per genotype, **p<0.01, ***p<0.001.

References

1. Mayeux R, Stern Y. Epidemiology of Alzheimer disease. Cold Spring Harb Perspect Med. 2012;2(8). Epub 2012/08/22. doi: 10.1101/cshperspect.a006239. PubMed PMID: 22908189; PubMed Central PMCID: PMCPMC3405821.
2. Tcw J, Goate AM. Genetics of beta-Amyloid Precursor Protein in Alzheimer's Disease. Cold Spring Harb Perspect Med. 2017;7(6). Epub 2016/12/23. doi: 10.1101/cshperspect.a024539. PubMed PMID: 28003277; PubMed Central PMCID: PMCPMC5453386.
3. Sherrington R, Rogaev EI, Liang Y, Rogaeva EA, Levesque G, Ikeda M, et al. Cloning of a gene bearing missense mutations in early-onset familial Alzheimer's disease. Nature. 1995;375(6534):754-60. Epub 1995/06/29. doi: 10.1038/375754a0. PubMed PMID: 7596406.
4. O'Brien RJ, Wong PC. Amyloid precursor protein processing and Alzheimer's disease. Annu Rev Neurosci. 2011;34:185-204. Epub 2011/04/05. doi: 10.1146/annurev-neuro-061010-113613. PubMed PMID: 21456963; PubMed Central PMCID: PMCPMC3174086.
5. Yan R, Bienkowski MJ, Shuck ME, Miao H, Tory MC, Pauley AM, et al. Membrane-anchored aspartyl protease with Alzheimer's disease beta-secretase activity. Nature. 1999;402(6761):533-7. Epub 1999/12/11. doi: 10.1038/990107. PubMed PMID: 10591213.

6. Passer B, Pellegrini L, Russo C, Siegel RM, Lenardo MJ, Schettini G, et al. Generation of an apoptotic intracellular peptide by gamma-secretase cleavage of Alzheimer's amyloid beta protein precursor. J Alzheimers Dis. 2000;2(3-4):289-301. doi: 10.3233/jad-2000-23-408. PubMed PMID: 12214090.
7. Yao W, Tambini MD, Liu X, D'Adamio L. Tuning of Glutamate, But Not GABA, Release by an Intrasynaptic Vesicle APP Domain Whose Function Can Be Modulated by beta- or alpha-Secretase Cleavage. J Neurosci. 2019;39(35):6992-7005. Epub 2019/06/27. doi: 10.1523/JNEUROSCI.0207-19.2019. PubMed PMID: 31235642; PubMed Central PMCID: PMCPMC6733572.
8. Tambini MD, Yao W, D'Adamio L. Facilitation of glutamate, but not GABA, release in Familial Alzheimer's APP mutant Knock-in rats with increased β-cleavage of APP. Aging Cell. 2019;18(6):e13033. doi: 10.1111/acel.13033.
9. Chew H, Solomon VA, Fonteh AN. Involvement of Lipids in Alzheimer's Disease Pathology and Potential Therapies. Front Physiol. 2020;11:598. Epub 2020/06/26. doi: 10.3389/fphys.2020.00598. PubMed PMID: 32581851; PubMed Central PMCID: PMCPMC7296164.
10. Strittmatter WJ, Saunders AM, Schmechel D, Pericak-Vance M, Enghild J, Salvesen GS, et al. Apolipoprotein E: high-avidity binding to beta-amyloid and increased frequency of type 4 allele in late-onset familial Alzheimer disease. Proc Natl Acad Sci U S A. 1993;90(5):1977-81. Epub 1993/03/01. doi: 10.1073/pnas.90.5.1977. PubMed PMID: 8446617; PubMed Central PMCID: PMCPMC46003.
11. Wang Y, Cella M, Mallinson K, Ulrich JD, Young KL, Robinette ML, et al. TREM2 lipid sensing sustains the microglial response in an Alzheimer's disease model. Cell. 2015;160(6):1061-71. Epub 2015/03/03. doi: 10.1016/j.cell.2015.01.049. PubMed PMID: 25728668; PubMed Central PMCID: PMCPMC4477963.
12. Piehler AP, Ozcurumez M, Kaminski WE. A-Subclass ATP-Binding Cassette Proteins in Brain Lipid Homeostasis and Neurodegeneration. Front Psychiatry. 2012;3:17. Epub 2012/03/10. doi: 10.3389/fpsyt.2012.00017. PubMed PMID: 22403555; PubMed Central PMCID: PMCPMC3293240.
13. Segawa K, Kurata S, Yanagihashi Y, Brummelkamp TR, Matsuda F, Nagata S. Caspase-mediated cleavage of phospholipid flippase for apoptotic phosphatidylserine exposure. Science. 2014;344(6188):1164-8. Epub 2014/06/07. doi: 10.1126/science.1252809. PubMed PMID: 24904167.
14. Takasugi N, Araya R, Kamikubo Y, Kaneshiro N, Imaoka R, Jin H, et al. TMEM30A is a candidate interacting partner for the beta-carboxyl-terminal fragment of amyloid-beta precursor protein in endosomes. PLoS One. 2018;13(8):e0200988. Epub 2018/08/08. doi: 10.1371/journal.pone.0200988. PubMed PMID: 30086173; PubMed Central PMCID: PMCPMC6080755.
15. Yang Y, Sun K, Liu W, Zhang L, Peng K, Zhang S, et al. Disruption of Tmem30a results in cerebellar ataxia and degeneration of Purkinje cells. Cell Death Dis. 2018;9(9):899. Epub 2018/09/07. doi: 10.1038/s41419-018-0938-6. PubMed PMID: 30185775; PubMed Central PMCID: PMCPMC6125289.
16. Zhang L, Yang Y, Li S, Zhang S, Zhu X, Tai Z, et al. Loss of Tmem30a leads to photoreceptor degeneration. Sci Rep. 2017;7(1):9296. Epub 2017/08/26. doi: 10.1038/s41598-017-09506-5. PubMed PMID: 28839191; PubMed Central PMCID: PMCPMC5571223.
17. Tambini MD, Norris KA, D'Adamio L. Opposite changes in APP processing and human Abeta levels in rats carrying either a protective or a pathogenic APP mutation. Elife. 2020;9. Epub 2020/02/06. doi: 10.7554/eLife.52612. PubMed PMID: 32022689; PubMed Central PMCID: PMCPMC7018507.
18. Olsson F, Schmidt S, Althoff V, Munter LM, Jin S, Rosqvist S, et al. Characterization of intermediate steps in amyloid beta (Abeta) production under near-native conditions. J Biol

Chem. 2014;289(3):1540-50. Epub 2013/11/15. doi: 10.1074/jbc.M113.498246. PubMed PMID: 24225948; PubMed Central PMCID: PMCPMC3894335.

19. Siegel G, Gerber H, Koch P, Bruestle O, Fraering PC, Rajendran L. The Alzheimer's Disease gamma-Secretase Generates Higher 42:40 Ratios for beta-Amyloid Than for p3 Peptides. Cell Rep. 2017;19(10):1967-76. Epub 2017/06/08. doi: 10.1016/j.celrep.2017.05.034. PubMed PMID: 28591569.

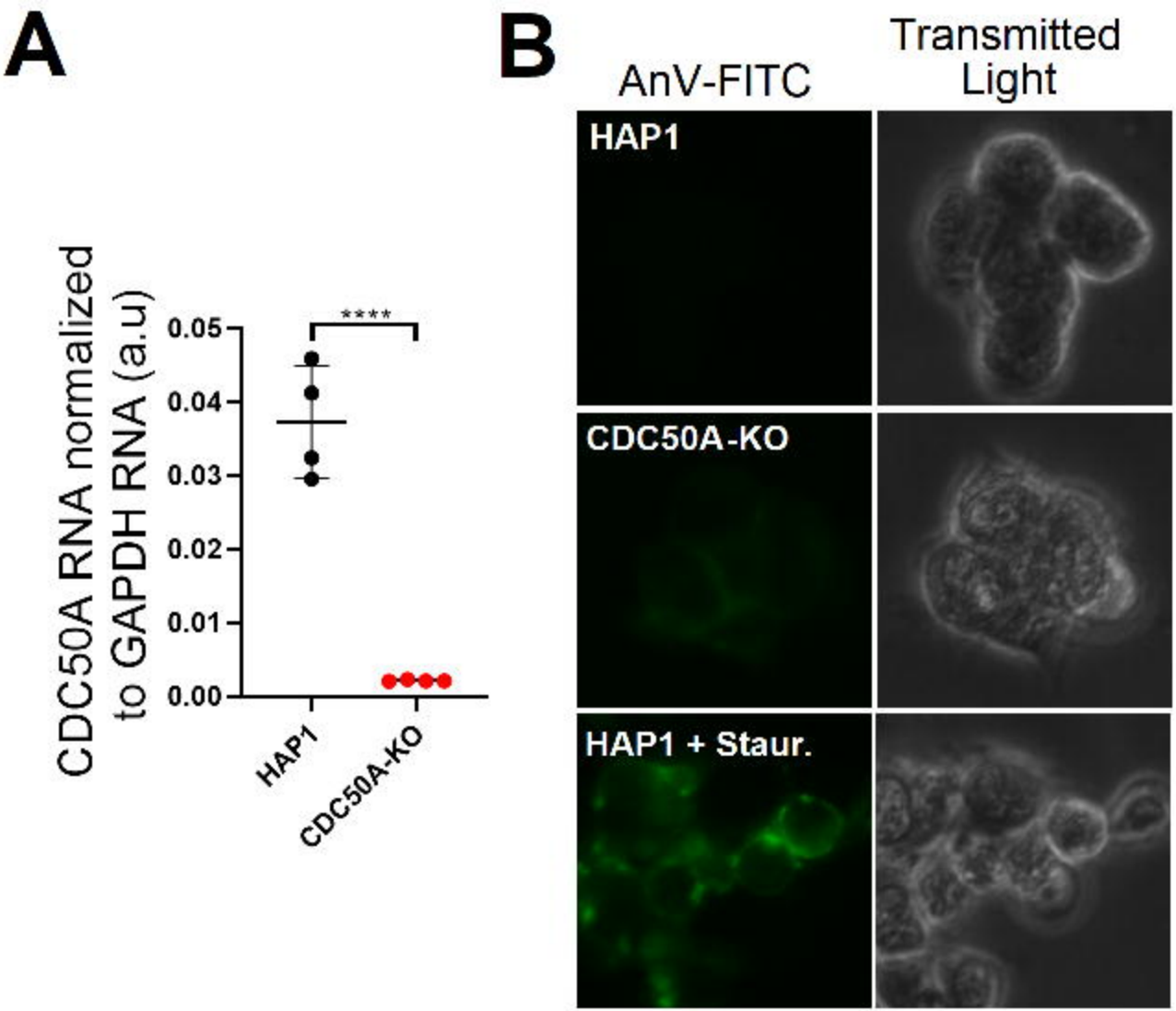
A
CDC50A RNA normalized to GAPDH RNA (a.u)
0.05
0.04
0.03
0.02
0.01
0.00
****
HAP1
CDC50A-KO
B
AnV-FITC
Transmitted Light
HAP1
CDC50A-KO
HAP1 + Staur.

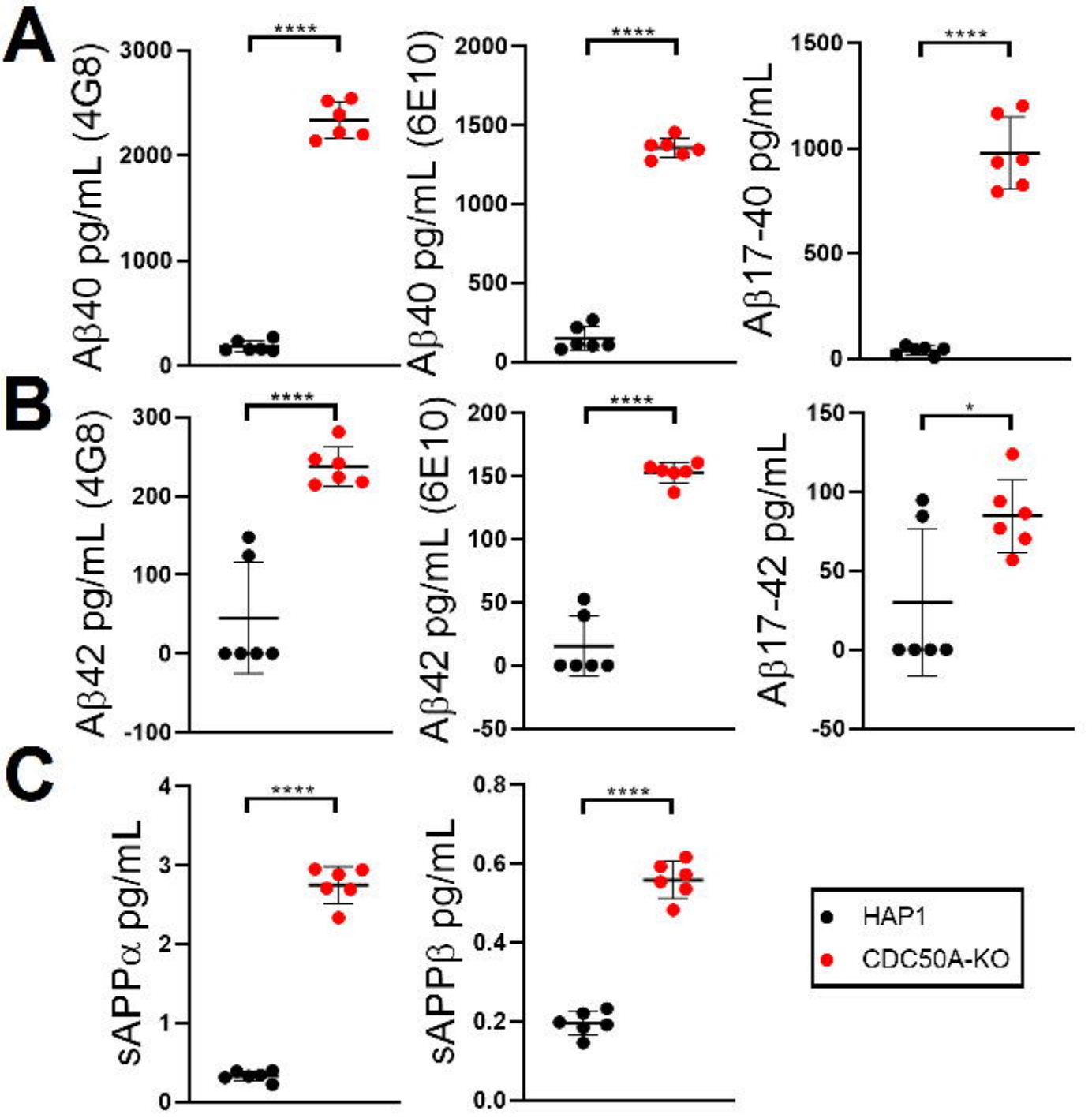
A
Aβ40 pg/mL (4G8)
3000
2000
1000
0
****
Aβ40 pg/mL (6E10)
2000
1500
1000
500
0
****
Aβ17-40 pg/mL
1500
1000
500
0
****
B
Aβ42 pg/mL (4G8)
300
200
100
0
-100
****
Aβ42 pg/mL (6E10)
200
150
100
50
0
-50
****
Aβ17-42 pg/mL
150
100
50
0
-50
*
C
sAPPα pg/mL
4
3
2
1
0
****
sAPPβ pg/mL
0.8
0.6
0.4
0.2
0.0
****
HAP1
CDC50A-KO

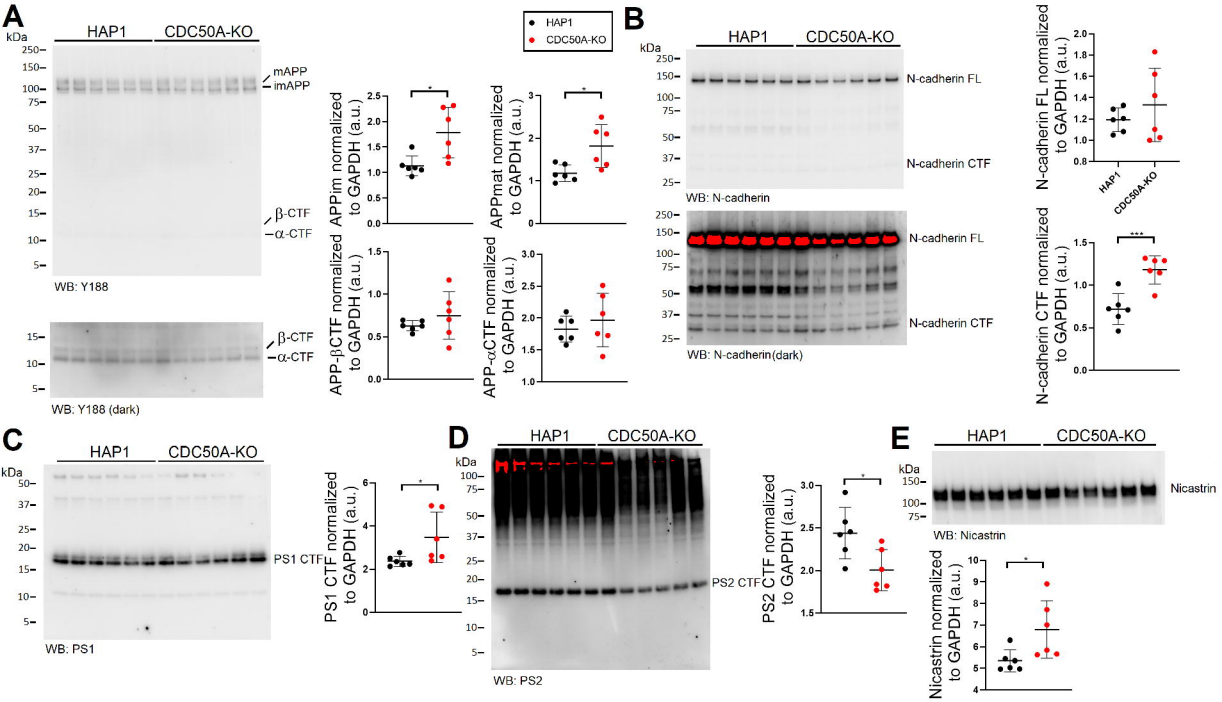
A
HAP1
CDC50A-KO
kDa
250
150
100
75
50
37
25
20
15
10
5
mAPP
imAPP
β-CTF
α-CTF
WB: Y188
WB: Y188 (dark)
HAP1
CDC50A-KO
APPim normalized to GAPDH (a.u.)
APPmat normalized to GAPDH (a.u.)
APP-βCTF normalized to GAPDH (a.u.)
APP-αCTF normalized to GAPDH (a.u.)
B
HAP1
CDC50A-KO
N-cadherin FL
N-cadherin CTF
WB: N-cadherin
WB: N-cadherin(dark)
N-cadherin FL normalized to GAPDH (a.u.)
N-cadherin CTF normalized to GAPDH (a.u.)
C
HAP1
CDC50A-KO
PS1 CTF
WB: PS1
PS1 CTF normalized to GAPDH (a.u.)
D
HAP1
CDC50A-KO
PS2 CTF
WB: PS2
PS2 CTF normalized to GAPDH (a.u.)
E
HAP1
CDC50A-KO
Nicastrin
WB: Nicastrin
Nicastrin normalized to GAPDH (a.u.)

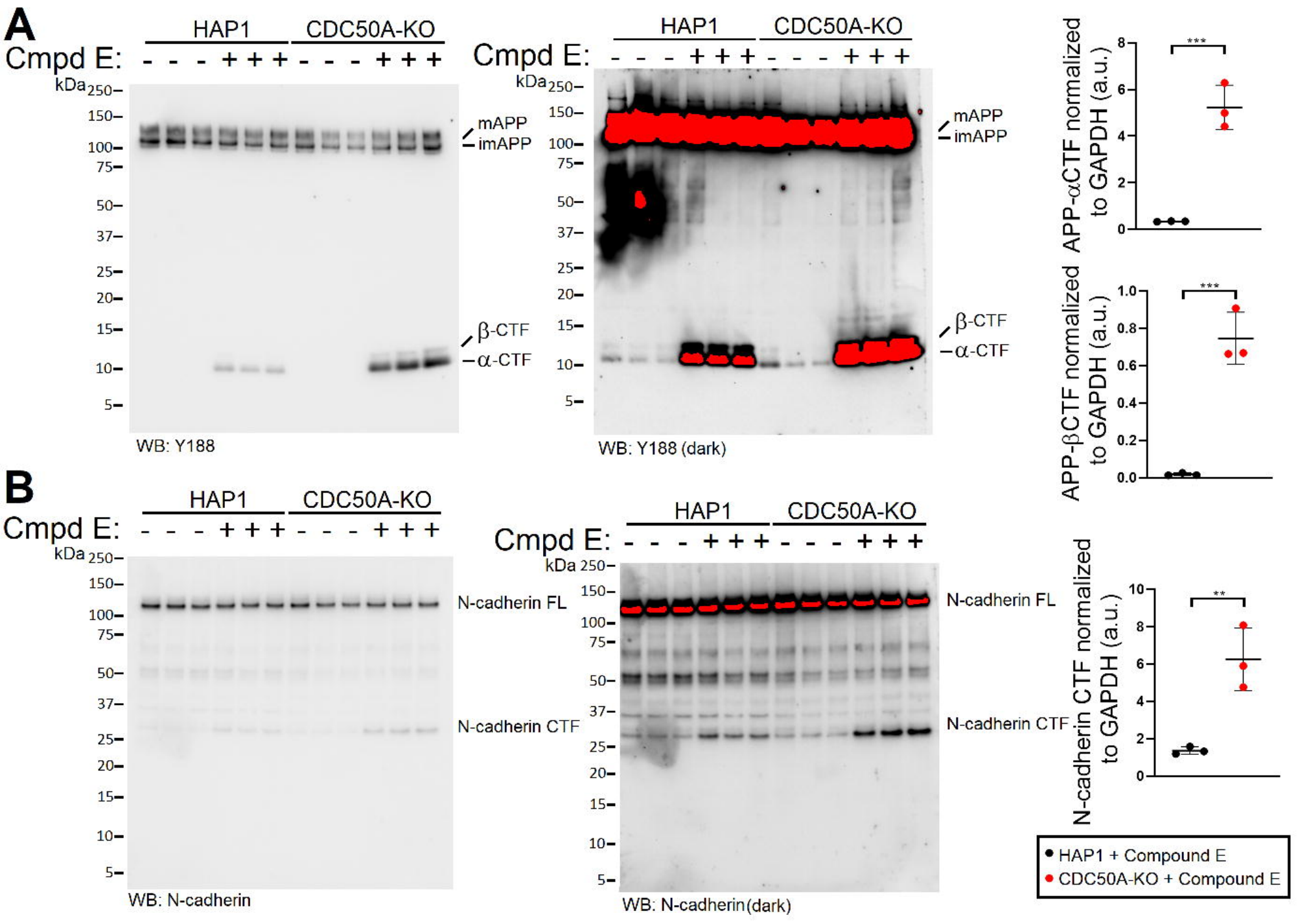
A
HAP1
CDC50A-KO
Cmpd E:
- - - + + + - - - + + +
kDa
250
150
100
75
50
37
25
20
15
10
5
mAPP
imAPP
β-CTF
α-CTF
WB: Y188
WB: Y188 (dark)
APP-αCTF normalized to GAPDH (a.u.)
APP-βCTF normalized to GAPDH (a.u.)
***
B
N-cadherin FL
N-cadherin CTF
WB: N-cadherin
WB: N-cadherin(dark)
N-cadherin CTF normalized to GAPDH (a.u.)
**
HAP1 + Compound E
CDC50A-KO + Compound E

Fig.3 Raw Blots

Order First 6 lanes -HAP1

Last 6 lanes -CDC50AKO

Nitrocellulose

Raw Blots w/Markers

APP-Y188

N-cadherin

PS1

PS2

Nicastrin

GAPDH

Note: GAPDH blot only used for purposes of quantification/normalization, image not present in Fig. 3

Fig.4 Raw Blots

Order First 6 lanes -HAP1 (3 untreated, 3 treated)

Last 6 lanes -CDC50AKO (3 untreated, 3 treated)

Nitrocellulose

Raw Blots w/Markers

APP-Y188

N-cadherin

GAPDH

Note: GAPDH blot only used for purposes of quantification/normalization, image not present in Fig. 4